

ROOAD: RELIS Offroad Odometry Analysis Dataset

George Chustz¹ and Srikanth Saripalli¹

Abstract—The development and implementation of visual-inertial odometry (VIO) has focused on structured environments, but interest in localization in off-road environments is growing. In this paper, we present the ROOAD which provides high-quality, time-synchronized off-road monocular visual-inertial data sequences to further the development of related research. We exhibit the 2-30x worse performance of two established VIO implementations, OpenVINS and VINS-Fusion, when stable, and the former is less prone to estimation divergences on our data sequences. The accuracy and repeatability of Kalibr’s IMU-camera extrinsics calibration tool is measured to be $\pm 1^\circ$ for orientation and $\pm 1\text{mm}$ at best (left-right) and $\pm 10\text{mm}$ (depth) at worst for position estimation in the camera frame. This novel dataset provides a new set of scenarios for researchers to design and test their localization algorithms on, as well as critical insights in the current performance of VIO off-road.

ROOAD Dataset: github.com/unmannedlab/ROOAD

I. INTRODUCTION

Localization is one of the fundamental problems in robotics. The development and analysis of localization algorithms requires detailed and carefully acquired datasets from a variety of scenarios and locations. There are many high-quality datasets which are publicly available; however, the majority of these do not provide off-road data. The research and development of autonomous vehicles is primarily focused on urban environments[1], [2], [3], [4], [5], [6], [7], highways, warehouses, indoor locations[8], [9], [10], simulations[11], and other developed areas.

Off road environments provide a different set of problems than urban environments. While there are far less pedestrians, vehicles, and rules, there are insects, animals, rocks, and plants. Ground vehicle dynamics change when driving over clay, dirt, sand, or mud. Obstacles should be avoided when on roads, but off road, some are navigable by the vehicle. Haze and cloud cover can change the lighting conditions and visibility dramatically. There are different LIDAR and camera features to track. The variety in texture of driving surfaces provides different excitation profiles for inertial sensors.

Visual-Inertial Odometry (VIO) is one such set of algorithms which estimate the local orientation and position of a vehicle using an Inertial-Measurement Unit (IMU) and cameras. VIO datasets need to be carefully acquired with special attention on the time stamping of images and IMU readings. While cameras and IMUs are relatively inexpensive sensors, acquiring accurate time stamps and performing time synchronization can be expensive and labor intensive.

¹J. Mike Walker '66 Department of Mechanical Engineering, Texas A&M University, College Station, TX 77843, USA {gchustz, ssaripalli}@tamu.edu



Fig. 1: Image of Clear Path’s Warthog Platform[12] at the testing site. This location is a dried mud pit within the Up-Down path.

In this work, we introduce RELIS Offroad Odometry Analysis Dataset (ROOAD) to contribute time-synchronized monocular VIO data to further the development of this field. The data sequences are recorded at a desert off-road testing field surrounding a sinkhole at the Texas A&M University System RELIS Campus (Fig. 3), using ClearPath’s Warthog[12] platform (Fig. 1) and IEEE-1588 (PTP)[13] to accurately time stamp the raw data from the sensor array. The performances of OpenVINS and VINS-Fusion are evaluated with respect to real time kinematic positioning (RTK) GPS ground truth, and the performance of the camera-IMU extrinsics calibration tool Kalibr is measured using the precision hatching on the camera slide (shown in Fig. 2). The major contributions of this work are as follows:

- We release six time stamped visual, inertial, and ground truth data sequences acquired while traversing off-road at the RELIS testing grounds.
- We demonstrate the performance of the state-of-the-art VIO implementation OpenVINS and VINS-Fusion on our off-road traversal data sequences.
- We validate the efficacy of the Kalibr camera-IMU cross calibration tool through the release and analysis of 11 additional calibration datasets with various relative horizontal position and yaw orientations between the camera and IMU.

II. RELATED WORK

A. Datasets

There is a large collection of publicly available autonomous vehicle traversal datasets for researchers to develop their work. There are plenty of high quality multi-modal urban data sets such as KITTI[2] and NuScenes[3], and other datasets focused only on images and point clouds for semantic segmentation (Cityscapes[4], BDD100K[5], Mapillary Vistas[6], Toronto-3D[1], and A2D2[7] which cannot be used

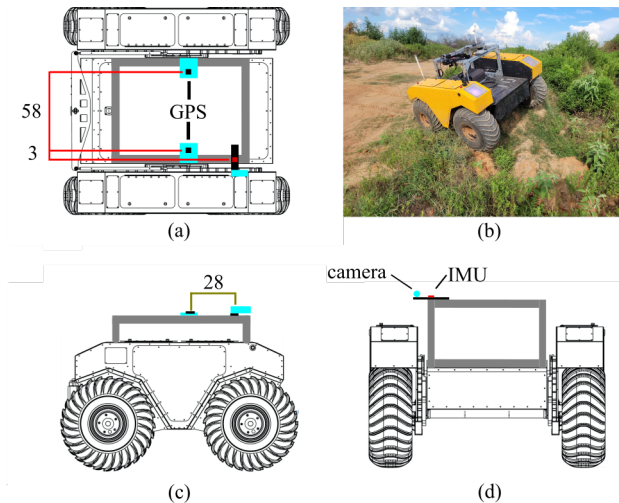


Fig. 2: Clearpath’s Warthog Platform[12] Configuration. Illustration of the dimensions and mounting positions of the sensors with respect to the Warthog’s top (a), side (c), and front (d) view. An image of the Warthog traversing a hill is included (b). (Units: cm)

for localization). Many VIO-centric datasets are acquired indoors such as TUM[8], UZH-FPV[9], and EuRoC[10]. Lastly, there are simulation-based data sets such as Tartan AIR[14].

There is a clear gap in the availability of off-road focused data sets. While the field is still growing, it is in its infancy when compared to the efforts put into collecting data for urban environments. Currently available high-quality offroad datasets include RUGD[15] and YCOR[16], and multi-modal data sets RELIS-3D[17] and Frieberg Forest dataset[18]. The development of autonomous vehicle technologies is dependent on both breadth and depth of available datasets. ROOAD extends the available data collection to this emerging area of autonomy.

B. Algorithms

Our contribution to autonomous navigation is centered on off-road VIO. There are several publicly available, state-of-the-art Visual(-inertial) Odometry implementations for researchers to test and extend. OKVIS[19], R-VIO[20], ROVIO[21], S-MSCKF[22], and ICE-BA[23] are all VIO implementations which have advanced this research area in the last five years, and recently VINS-Fusion[24] and OpenVINS[25] have presented state-of-the-art implementations of VIO using different approaches. VINS-Fusion utilizes optimization-based estimation whereas OpenVINS uses a Kalman Filter-based approach. These implementations have been extensively tested in urban and indoors environments, and in this paper their performance is exhibited in off-road scenarios.

III. SENSOR SETUP AND CALIBRATION

A. Sensors

The acquisition of VIO-centric data necessitated an IMU with adequate noise density characteristics and a camera which allows for time stamping of images. The sensor set is labeled with dimensions in Fig. 2 and consists of the following sensors:

- 1 × B/W Camera: Basler acA1920-50gc camera with 8mm/F1.8 Edmund Optics lens, resolution 1920x1200, 30 Hz, 1ms exposure
- 1 × IMU: Vectornav VN-300 INS at 400 Hz (GPS denied)
- 1 × GPS: ArduSimple Differential Heading with RTK kit, 10 Hz, local ArduSimple Basestation, all ZED-F9P GPS Modules

For the data collection, a computer with Power Over Ethernet (POE) and PTP capable network interface card is mounted to the top of the Warthog. The calibration, OpenVINS and VINS-Fusion implementations, and Kalibr evaluations are performed offline on a separate computer. Both computers run Ubuntu 20.04 (64 bit) and ROS Noetic for data collection and evaluation.

B. Synchronization

Using the Linux PTP package for Ubuntu, a boundary clock is established using the system’s clock as the grandmaster and the network interface as the slave. The Basler Pylon Camera ROS driver was modified¹ to use PTP time stamps from the camera itself. Unfortunately, the Vectornav IMU does not support PTP time synchronization, and the IMU’s and system’s clocks diverge over time. A one-dimensional Kalman filter[26] is used² to correct the discrepancy between the IMU and system clock. The time synchronization is verified prior and during every data collection run by monitoring the end-to-end latencies of the IMU and camera time stamps with respect to the system time.

C. Camera Calibration

Both OpenVINS, VINS-Fusion, and Kalibr support the pin-hole projection and radial-tangential distortion models. The pin-hole projection model assumes that the camera is projecting three-dimensional points onto an image plane through a singular point at the camera’s aperture, and the radial tangential distortion model assumes that the lens distortion and sensor-lens misalignment can be modeled using polynomial approximation. The pinhole camera model matrix and the radial-tangential distortion parameters are estimated using the Kalibr toolbox. For the benchmarks and evaluations, we assume that the pin-hole model for the camera calibration and radial-tangential distortion model are adequate.

¹<https://github.com/unmannedlab/pylon-ros-camera>

²https://github.com/unmannedlab/vectornav/tree/feature/resync_imu

D. IMU Calibration

For the IMU calibration, the Kalibr Allan toolbox determines the noise density and uses Allan Variance to estimate the random walk of the angle rate gyroscope and linear accelerometer. The data used to calculate the Allan Variance is approximately six-hours of stationary IMU data at 400 Hz. The linear acceleration noise density σ_a and random walk σ_{aw} is estimated to be $1.1 \times 10^{-4} m/s^2/\sqrt{Hz}$ and $3.2 \times 10^{-5} m/s^3/\sqrt{Hz}$, respectively, and the rate gyroscope noise density σ_g and random walk σ_{gw} is $6.5 \times 10^{-5} rad/s/\sqrt{Hz}$ and $5.0 \times 10^{-6} rad/s^2/\sqrt{Hz}$, respectively.

E. IMU & Camera Calibration

The IMU-Camera cross calibration estimates the translation and orientation transform between the IMU and camera as well as the potential time offset between the camera and IMU. This cross calibration is performed using Kalibr calibrate camera-IMU tool. The estimate is verified using hand measured values and the efficacy of Kalibr’s estimation ability is tabulated in Table IV.

F. Ground Truth GPS and Heading

Ardusimple’s simpleRTK2B and simpleRTK2Blite breakout boards[27] are used to acquire ground truth differential RTK GPS and heading. For this dataset, RTK GPS coordinates consisting of latitude, longitude, height are required to analyze the estimated position, and heading from RTK differential GPS is recorded to analyze orientation estimation performance. The base station is a singular GPS receiver, which surveys its location using the assumption that its position is stationary. The base station is able to transmit corrections to the differential GPS pair over 900MHz telemetry radios included in the ArduSimple kit. A single simpleRTK2B board acts as an RTK base station while a simpleRTK2B and a simpleRTK2Blite are mounted on the Warthog with GPS antennas placed as shown in Fig. 2. The Warthog’s simpleRTK2Blite board is in a ”moving basestation” configuration which receives RTK coordinates from the stationary base station. The Warthog’s simpleRTK2B board is in a ”rover” configuration which is determining the craft’s GPS position and heading based on the relative heading of the simpleRTK2Blite’s GPS antenna.

IV. DATASET

A. Data Description

ROOAD includes six sequences of Visual-Inertial data along three paths (shown in Fig. 3). The location presents desert conditions including shrubs, hills, and various elevations of terrain. The terrain of the testing field surrounds a sinkhole at the RELLIS Campus. The first path, ”gravel,” is acquired by driving on a stretch of gravel, then driving off road adjacent to the path back to the starting point. The second path, ”rim,” is focused on a path which approaches the edge of the sinkhole before turning and returning back to the starting location. The final path, ”updown,” includes traversal along a dirt path, descent onto an eroded plateau, and return to the starting path. Each of these paths are

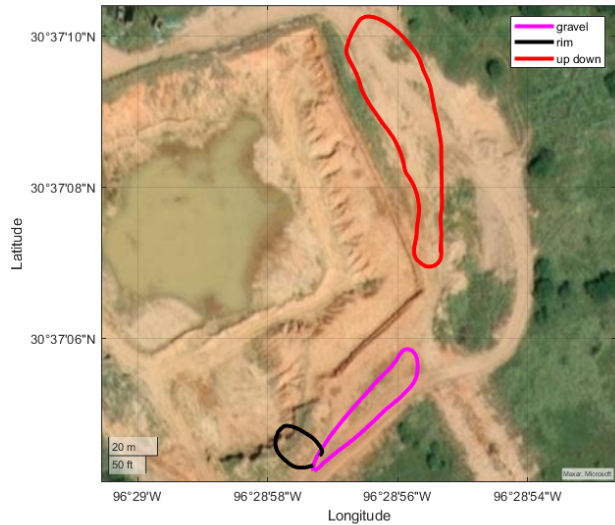


Fig. 3: Satellite imagery of the testing ground with the ground truth path coordinates overlaid.

recorded once at around 10 AM and again at around 7 PM local time to capture different lighting scenarios. The image, IMU, and GPS message counts for the individual datasets are given in Table I and the max achieved excitations are shown in Table II. ROOAD contains some large excitations in excess of 3g’s and large angle rates measured at the IMU to test the capabilities of VIO implementation. ROOAD is comprised of over 6,000 GPS waypoints, 20,000 images, and 250,000 IMU readings across its traversal data sequences to provide visual-inertial algorithm developers a new test-bed for their work.

TABLE I: ROOAD data sequences overview.

Data Sequence	Dist. (m)	Images	IMU Messages	RTK GPS Messages	Time Period
rt4_gravel	135.8	3433	45765	1144	evening
rt4_rim	51.9	2085	27804	695	evening
rt4_updown	241.9	5364	71519	1787	evening
rt5_gravel	132.4	2980	39740	994	morning
rt5_rim	51.6	2257	30098	748	morning
rt5_updown	221.7	4447	59290	1481	morning

Additionally, there are 11 camera-IMU cross calibration datasets provided. For each of the datasets in this group, the camera is either translated along the IMU’s x-axis while the rotation is held constant or rotated about the IMU’s z-axis while the orientation is held constant. Since Kalibr’s calibration tools are used widely within the research community, the validation of these tools would provide useful feedback and consideration for those who are using Kalibr or developing counterparts. The Kalibr calibration analysis shows adequate repeatability and accuracy among the different configurations tested.

V. BENCHMARKS, EVALUATION METRICS AND EXPERIMENTS

The analysis of the OpenVINS and VINS-Fusion trajectories consists of comparing the ground truth trajectories of

TABLE II: Maximum linear and angular excitation per dataset. The largest excitation of each column is bolded. (Units: m/s² and rad/s)

Data Sequence	\ddot{x}_{max}	\ddot{y}_{max}	\ddot{z}_{max}	$\omega_{x,max}$	$\omega_{y,max}$	$\omega_{z,max}$
rt4_gravel	-22.6	7.0	7.5	0.4	-0.7	-0.6
rt4_rim	-10.5	6.4	-4.9	0.5	-0.6	0.5
rt4_updown	31.9	-11.2	-15.5	0.8	1.4	-0.6
rt5_gravel	-27.0	-13.7	11.9	0.9	1.0	-0.6
rt5_rim	-11.0	7.5	-5.1	0.8	0.6	0.4
rt5_updown	-30.8	-20.5	-21.3	2.1	1.4	-0.8

TABLE III: Median relative pose error of OpenVINS (OV) & VINS-Fusion (VF) for the provided datasets. Bolded values are the better of the two algorithms of each metric of each dataset.

File Name	8m OV	8m VF	24m OV	24m VF	40m OV	40m VF
rt4_gravel	1.9°/0.8m	2.5°/0.7m	2.7°/2.4m	3.1°/1.6m	5.3°/3.6m	4.4°/2.7m
rt4_rim	6.0°/1.5m	6.8°/4.4m	9.6°/3.0m	14.0°/19.4m	9.4°/1.6m	N/A / N/A ¹
rt4_updown	3.5°/0.9m	3.7°/0.8m	5.7°/2.5m	6.0°/1.9m	8.1°/3.7m	8.5°/2.7m
rt5_gravel	2.2°/0.6m	2.7°/0.8m	3.4°/1.8m	4.7°/2.0m	6.0°/2.8m	7.8°/3.1m
rt5_rim	5.8°/1.3m	6.5°/247.6m	9.7°/2.7m	11.8°/736.5m	8.2°/2.4m	N/A / N/A ¹
rt5_updown	3.6°/0.8m	3.8°/0.8m	6.4°/1.8m	6.7°/1.8m	9.1°/2.4m	9.5°/2.3m

¹ Divergent values caused errors when calculating the relative pose error.

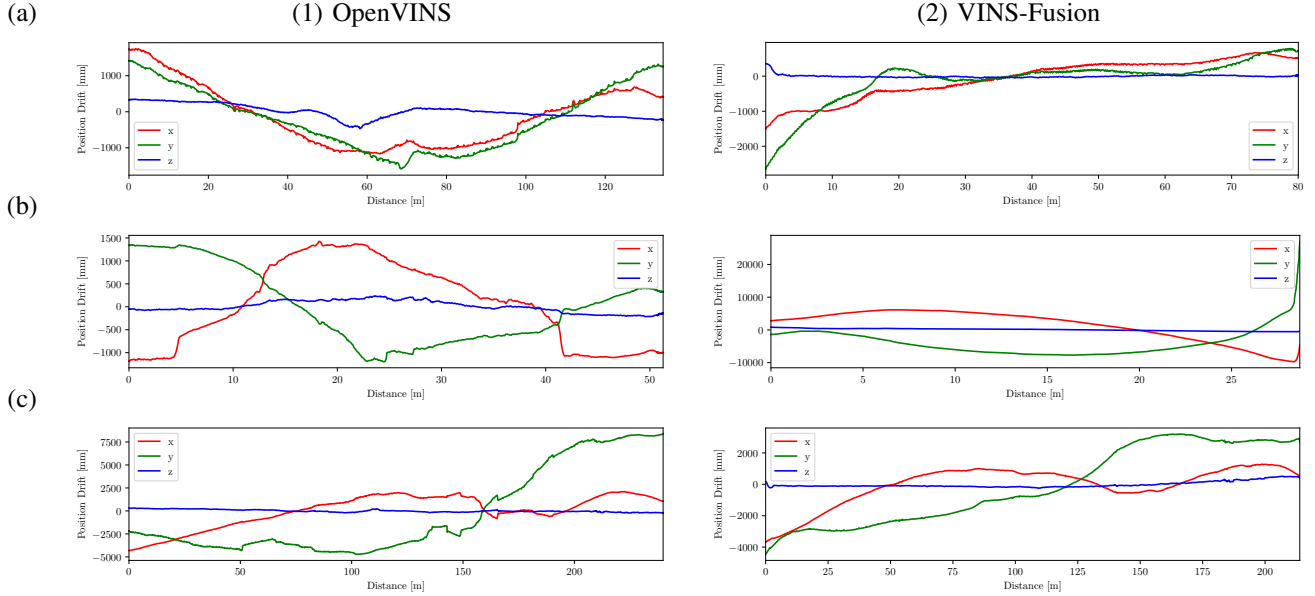


Fig. 4: Comparison of translation errors. (a) represents the gravel path, (b) represents the rim path, and (c) represents the up-down path of the rt4 (evening) data sequences. (Units: mm/m)

TABLE IV: Results of Kalibr Horizontal Trials. All other rotational and translational modes are fixed. The expected y and z relative measurements are 75mm and -30mm, respectively. (Units: mm)

Slider Measurement	X	Y	Z
120	119	68	-66
90	89	67	-68
60	59	67	-71
-70	-69	70	-85
-100	-99	68	-86
-130	-129	71	-90

the data sequences with the aligned VIO estimated trajectories. The ground truth RTK differential GPS is capable of measuring latitude, longitude, height, and heading, but is unable capture pitch and roll measurements. Northing

TABLE V: Results of Kalibr Yaw Rotation Trials. All other rotational and translational modes are fixed. The measured x and y Euler Angles are -90° and 0°, respectively. (Units: degrees)

Measured Z-Angle	X	Y	Z
-125	-90.3	-0.1	-125.3
-110	-90.2	-0.4	-109.5
-95	-90.4	-2.9	-92.6
-80	-89.9	-0.9	-79.5
-65	-89.7	-1.0	-64.9

and Easting position components are extracted in meters using the Universal-Transverse Mercator (UTM) python package[28]. The heading measurements are converted into unit quaternions for comparison in OpenVINS Evaluation toolkit.

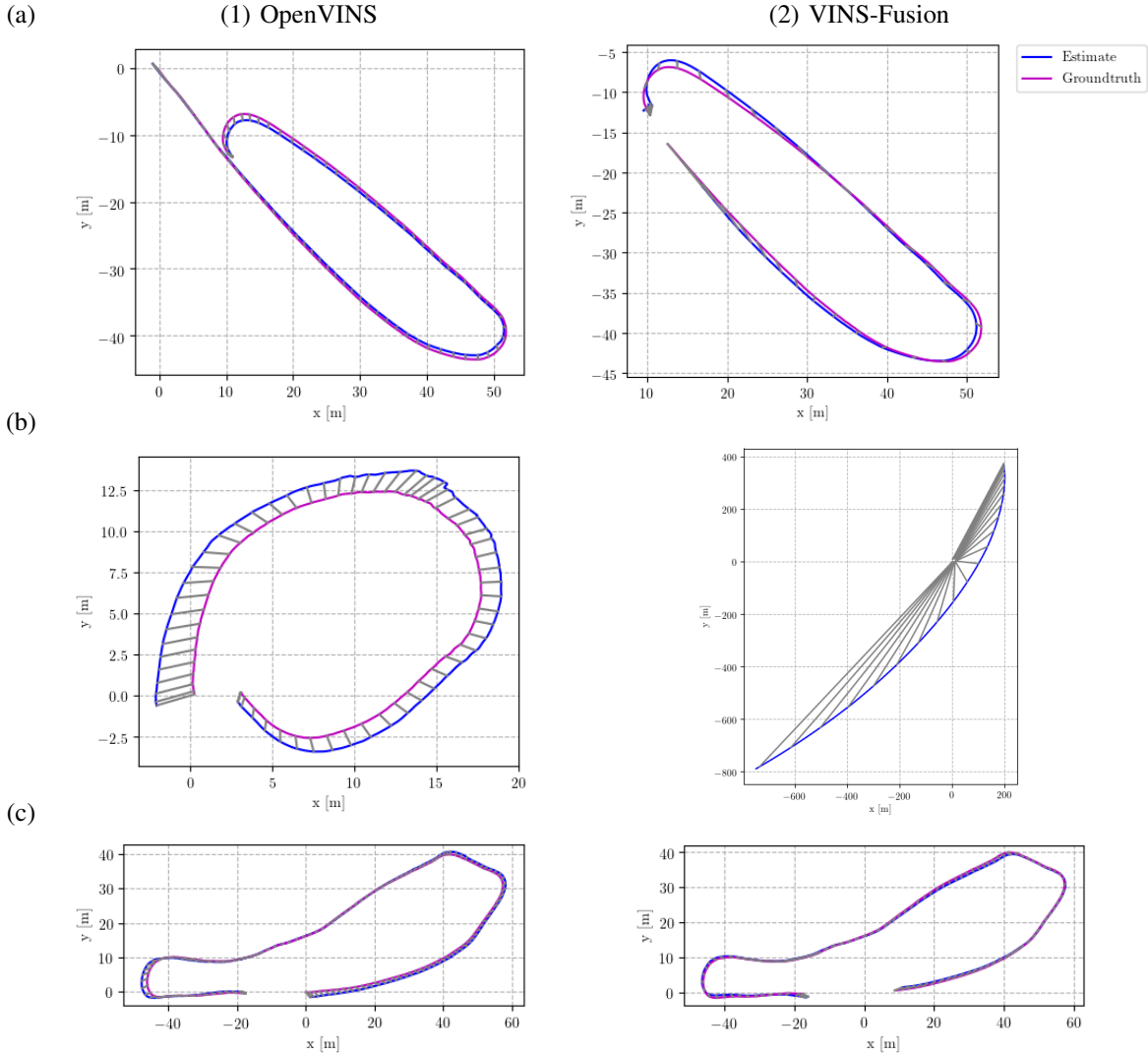


Fig. 5: Comparison of trajectory estimates aligned to ground truth GPS of the (a) gravel path, (b) rim path, and (c) the up-down path for OpenVINS (1) and VINS-Fusion (2). The rim path was the most difficult for OpenVINS and VINS-Fusion was highly divergent on it. The gray lines between the estimated trajectory and the ground truth trajectory show the error after the trajectories have been aligned. (Units: m)

OpenVINS and VINS-Fusion are selected for trajectory estimation of the collected data because they represent the dichotomy of strategies of VIO and are state-of-the-art implementations. OpenVINS uses a multi-state constraint sliding Kalman Filter (MSCKF) for estimation with Simultaneous Localization and Mapping (SLAM) feature tracking for loop-closure[25]. VINS-Fusion uses non-linear optimization based system for pose estimation with loop detection and pose graph optimization for global consistency[24]. These algorithms have shown that they perform adequately across indoor environments[25]. The rt4 and rt5 configurations for the implementations of OpenVINS and VINS-Fusion are provided on the ROOAD website.

The OpenVINS Evaluation toolkit includes integration of the trajectory estimation performance metrics Absolute Trajectory Error (ATE) and Relative Pose Error (RPE)[25], [29]. The ATE simply measures the error between the given

ground truth trajectory $x_{k,i}$ and the estimated trajectory $\hat{x}_{k,i}^+$ after the best alignment transformation has been performed for K pose measurements over N runs (exhibited in Fig. 5).

$$e_{ATE} = \frac{1}{N} \sum_{i=1}^N \sqrt{\frac{1}{K} \sum_{k=1}^K \|x_{k,i} - \hat{x}_{k,i}^+\|_2^2}$$

ATE is a helpful metric when comparing the performance of one algorithm to another, but it is missing key insights of how the trajectory estimate is behaving for different measurement periods and traversal lengths. RPE compares the relative poses between the estimate and the ground truth to compare how the trajectory diverges over different segments of lengths $D = [d_1, d_2, \dots, d_i]$ of the estimated trajectory. The relative pose error for D_i segments is the magnitude of the error between the ground truth pose evolution $\tilde{x}_{k,i}$ and the estimated pose evolution $\hat{\tilde{x}}_{k,i}$ over length d_i .

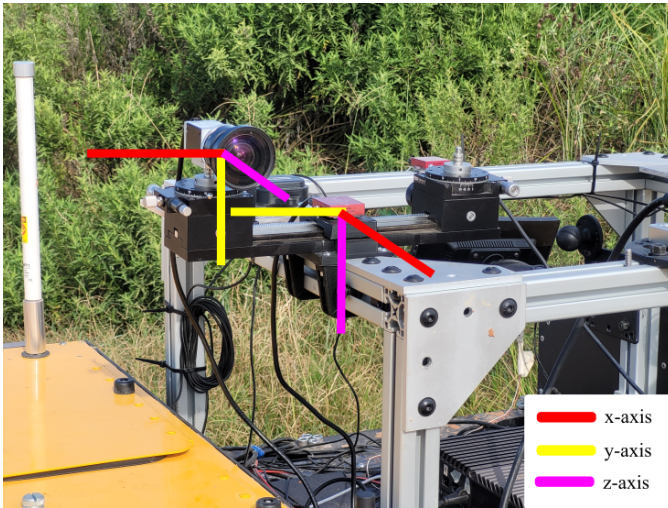


Fig. 6: Warthog Sensor Orientation. Illustration of the co-ordinate axes of the IMU and camera. The camera’s sensor is located at approximately 3, 13, and -7.5 cm on the x, y, and z-axes of the IMU co-ordinate system, respectively.

$$\tilde{x}_r = x_k - x_{k+d_i}$$

$$e_{RPE,d_i} = \frac{1}{D_i} \sum_{k=1}^{D_i} \|\tilde{x}_{k,i} - \hat{x}_{k,i}\|_2^2$$

Using the ATE and RPE metrics, OpenVINS shows higher stability and consistency in our off-road scenario, but VINS-Fusion out-performs OpenVINS in certain segments. The Table III shows the RPE performance of OpenVINS and VINS-Fusion side-by-side. VINS-Fusion has lower translational RPE in rt4 gravel and both up-down datasets and OpenVINS has lower orientation RPE in those datasets. OpenVINS out-performs VINS-Fusion on all other datasets. Particularly, the rim datasets demonstrate a challenging scenario for the algorithms, and VINS-Fusion demonstrates large estimation divergences. Over 24 meter segments, OpenVINS has minimum orientation and translation RPE of 2.7° and 1.8m, respectively, while VINS-Fusion achieves 3.1° and 1.6m, respectively. OpenVINS demonstrates 3.1-9.4x higher orientation and 9.1-37x higher position RPE and VINS-Fusion achieves (on non-diverging runs) 2-7.5x higher orientation and 11-30x higher position RPE than their corresponding segment length runs on the EuRoC dataset[25]. Fig. 4 exhibits the ATE for in the x, y, and z directions over the trajectories’ length for OpenVINS and VINS-Fusion across the evening (rt4) datasets, and Fig. 5 shows the error between the aligned trajectories for the morning (rt5) datasets.

Many VIO research applications have turned to Kalibr as the de facto camera-IMU extrinsics estimator. To measure the efficacy of Kalibr camera-IMU extrinsic calibration, several calibration sequences are provided with measured camera linear and angular positions using the camera rail hatching and orientations shown in Fig. 6. This position and orientation estimation of the camera-IMU extrinsics is performed

using Kalibr’s calibrate camera-IMU tool. Processing these sequences in Kalibr results in Table IV and V. Kalibr shows strong repeatability and accuracy within $\pm 1^\circ$ for rotational measurements and $\pm 1\text{mm}$ for the x and y measurements in the camera frame. The linear estimation of depth (z) axis of the camera is the least accurate with an average error of 47mm and a measurement standard deviation of 10mm. It is important to note that it is difficult to accurately hand measure the exact position of the aperture and height of the camera sensor with respect to the IMU’s exact sensor location when these sensors are enclosed, which grants more confidence to Kalibr’s results.

VI. SUMMARY AND FUTURE WORK

In this paper, we present ROOAD, a collection of off-road monocular visual-inertial data sequences, to contribute to the research community. We demonstrate that two state-of-the-art VIO implementations, OpenVINS and VINS-Fusion, present promise but their performance is lacking when compared to their indoors capabilities. OpenVINS exhibits consistent trajectory estimation performance across our data sequences when compared to VINS-Fusion which diverges heavily in our ”rim” data sequences. VINS-Fusion does outperform OpenVINS in the positional estimation on the rt4 gravel and both of our up-down data sets, but OpenVINS outperforms VINS-Fusion in all other scenarios. Both implementations demonstrate between 200-3000% higher error on our off-road dataset when compared to the EuRoC dataset. OpenVINS demonstrates a maximum 40m segment RPE of 9.4° and 3.7m while VINS-Fusion, when stable, achieves 9.5° and 3.1m. This performance gap shows that there is not a direct transference of VIO capabilities from developed to off-road environments and that there is opportunity for further improvement.

Additionally, we validate the efficacy of Kalibr camera-IMU extrinsics calibration tool by collecting multiple calibration datasets at different linear and angular camera-IMU offsets. Kalibr has exceeded our expectations with accuracy and repeatability within 1° for our angular measurements and adequate estimation along its linear axes with the best of $\pm 1\text{mm}$ on its x-axis (left-right) and at worst $\pm 10\text{mm}$ on z-axis (depth) from the camera frame.

In the future, we consider extending our off-road data collection to include similarly PTP time-stamped stereo cameras and LIDAR(s). In order to capture more scenarios, we would like to attach this sensor suite to multiple vehicles for similar data collection runs with their different geometry, dynamics, and excitation profiles. We are also interested in the effects of varying exposure times in state estimation and allowing for automatic exposure control by the camera to adjust for the varied lighting conditions outdoors.

REFERENCES

- [1] W. Tan, N. Qin, L. Ma, Y. Li, J. Du, G. Cai, K. Yang, and J. Li, ”Toronto-3D: A Large-scale Mobile LiDAR Dataset for Semantic Segmentation of Urban Roadways,” pp. 202–203, 2020. [Online]. Available: <http://arxiv.org/abs/2003.08284>

- [2] A. Geiger, P. Lenz, C. Stiller, and R. Urtasun, "Vision meets robotics: The kitti dataset," *International Journal of Robotics Research (IJRR)*, 2013.
- [3] H. Caesar, V. Bankiti, A. H. Lang, S. Vora, V. E. Liong, Q. Xu, A. Krishnan, Y. Pan, G. Baldan, and O. Beijbom, "nuScenes: A multimodal dataset for autonomous driving," mar 2019. [Online]. Available: <http://arxiv.org/abs/1903.11027>
- [4] M. Cordts, M. Omran, S. Ramos, T. Rehfeld, M. Enzweiler, R. Benenson, U. Franke, S. Roth, and B. Schiele, "The Cityscapes Dataset for Semantic Urban Scene Understanding," in *Proc. IEEE Comput. Soc. Conf. Comput. Vis. Pattern Recognit.*, vol. 2016-December. IEEE Computer Society, dec 2016, pp. 3213–3223. [Online]. Available: <http://arxiv.org/abs/1604.01685>
- [5] F. Yu, H. Chen, X. Wang, W. Xian, Y. Chen, F. Liu, V. Madhavan, and T. Darrell, "BDD100K: A Diverse Driving Dataset for Heterogeneous Multitask Learning," may 2018. [Online]. Available: <http://arxiv.org/abs/1805.04687>
- [6] G. Neuhold, T. Ollmann, S. R. Buló, and P. Kotschieder, "The Mappillary Vistas Dataset for Semantic Understanding of Street Scenes," in *Proc. IEEE Int. Conf. Comput. Vis.*, vol. 2017-October. Institute of Electrical and Electronics Engineers Inc., dec 2017, pp. 5000–5009.
- [7] J. Geyer, Y. Kassahun, M. Mahmudi, X. Ricou, R. Durgesh, A. S. Chung, L. Hauswald, V. H. Pham, M. Mühlegg, S. Dorn, T. Fernandez, M. Jänicke, S. Mirashi, C. Savani, M. Sturm, O. Vorobiov, M. Oelker, S. Garreis, and P. Schuberth, "A2D2: Audi Autonomous Driving Dataset," apr 2020. [Online]. Available: <http://arxiv.org/abs/2004.06320>
- [8] J. Sturm, N. Engelhard, F. Endres, W. Burgard, and D. Cremers, "A benchmark for the evaluation of rgb-d slam systems," in *Proc. of the International Conference on Intelligent Robot Systems (IROS)*, Oct. 2012.
- [9] J. Delmerico, T. Cieslewski, H. Rebecq, M. Faessler, and D. Scaramuzza, "Are we ready for autonomous drone racing? the UZH-FPV drone racing dataset," in *IEEE Int. Conf. Robot. Autom. (ICRA)*, 2019.
- [10] M. Burri, J. Nikolic, P. Gohl, T. Schneider, J. Rehder, S. Omari, M. W. Achtelik, and R. Siegwart, "The euroc micro aerial vehicle datasets," *The International Journal of Robotics Research*, 2016. [Online]. Available: <http://ijr.sagepub.com/content/early/2016/01/21/0278364915620033.abstract>
- [11] J. Wang, K. Sun, T. Cheng, B. Jiang, C. Deng, Y. Zhao, D. Liu, Y. Mu, M. Tan, X. Wang, W. Liu, and B. Xiao, "Deep high-resolution representation learning for visual recognition," *TPAMI*, 2019.
- [12] C. Robotics, "Warthog unmanned ground vehicle," Accessed Sep. 14, 2021 [Online]. [Online]. Available: <https://clearpathrobotics.com/warthog-unmanned-ground-vehicle-robot/>
- [13] "Ieee standard for a precision clock synchronization protocol for networked measurement and control systems," IEEE 1588-2019, 2020.
- [14] W. Wang, D. Zhu, X. Wang, Y. Hu, Y. Qiu, C. Wang, Y. Hu, A. Kapoor, and S. Scherer, "Tartanair: A dataset to push the limits of visual slam," 2020.
- [15] M. Wigness, S. Eum, J. G. Rogers, D. Han, and H. Kwon, "A rugd dataset for autonomous navigation and visual perception in unstructured outdoor environments," in *IROS*, 2019.
- [16] D. Maturana, P.-W. Chou, M. Uenoyama, and S. Scherer, "Real-Time Semantic Mapping for Autonomous Off-Road Navigation," in *F. Serv. Robot.*, M. Hutter and R. Siegwart, Eds. Cham: Springer International Publishing, 2018, pp. 335–350.
- [17] P. Jiang, P. Osteen, M. Wigness, and S. Saripalli, "Rellis-3d dataset: Data, benchmarks and analysis," 2020.
- [18] A. Valada, G. Oliveira, T. Brox, and W. Burgard, "Deep multispectral semantic scene understanding of forested environments using multi-modal fusion," in *ISER*, 2016.
- [19] S. Leutenegger, S. Lynen, M. Bosse, R. Siegwart, and P. Furgale, "Keyframe-based visual-inertial odometry using nonlinear optimization," *The International Journal of Robotics Research*, vol. 34, no. 3, pp. 314–334, 2015.
- [20] Z. Huai and G. Huang, "Robocentric visual-inertial odometry," *The International Journal of Robotics Research*, 2019. [Online]. Available: <https://journals.sagepub.com/doi/10.1177/0278364919853361>
- [21] M. Bloesch, M. Burri, S. Omari, M. Hutter, and R. Siegwart, "Iterated extended kalman filter based visual-inertial odometry using direct photometric feedback," *The International Journal of Robotics Research*, vol. 36, no. 10, pp. 1053–1072, 2017. [Online]. Available: <https://doi.org/10.1177/0278364917728574>
- [22] K. Sun, K. Mohta, B. Pfrommer, M. Watterson, S. Liu, Y. Mulgaonkar, C. J. Taylor, and V. Kumar, "Robust stereo visual inertial odometry for fast autonomous flight," 2018.
- [23] H. Liu, M. Chen, G. Zhang, H. Bao, and Y. Bao, "Ice-ba: Incremental, consistent and efficient bundle adjustment for visual-inertial slam," in *Proceedings of the IEEE Conference on Computer Vision and Pattern Recognition*, 2018, pp. 1974–1982.
- [24] T. Qin, S. Cao, J. Pan, and S. Shen, "A general optimization-based framework for global pose estimation with multiple sensors," 2019.
- [25] P. Geneva, K. Eickenhoff, W. Lee, Y. Yang, and G. Huang, "OpenVINS: A research platform for visual-inertial estimation," in *Proc. of the IEEE International Conference on Robotics and Automation*, Paris, France, 2020.
- [26] A. English, P. Ross, D. Ball, B. Ucpocroft, and P. Corke, "Triggersync: A time synchronisation tool," in *2015 IEEE International Conference on Robotics and Automation (ICRA)*, 2015, pp. 6220–6226.
- [27] ArduSimple, "Rtk starter kits," Accessed Sep. 14, 2021 [Online]. [Online]. Available: <https://www.ardusimple.com/rtk-starter-kits/>
- [28] T. Bieniek, "Bidirectional utm-wgs84 converter for python," 2020. [Online]. Available: <https://pypi.org/project/utm/>
- [29] Z. Zhang and D. Scaramuzza, "A tutorial on quantitative trajectory evaluation for visual(-inertial) odometry," in *IEEE/RSJ Int. Conf. Intell. Robot. Syst. (IROS)*, 2018.